

DOA Estimation for Hybrid Massive MIMO Systems using Mixed-ADCs: Performance Loss and Energy Efficiency

Baihua Shi, Rongen Dong, Qijuan Jie, Lingling Zhu, Feng Shu, and Jiangzhou Wang, *Fellow, IEEE*

Abstract—Due to the power consumption and high circuit cost in antenna arrays, the practical application of massive multiple-input multiple-output (MIMO) in the sixth generation (6G) and future wireless networks is still challenging. Employing low-resolution analog-to-digital converters (ADCs) and hybrid analog and digital (HAD) structure is two low-cost choice with acceptable performance loss. In this paper, the combination of the mixed-ADC architecture and HAD structure employed at receiver is proposed for direction of arrival (DOA) estimation, which will be applied to the beamforming tracking and alignment in 6G. By adopting the additive quantization noise model, the exact closed-form expression of the Cramér-Rao lower bound (CRLB) for the HAD architecture with mixed-ADCs is derived. Moreover, the closed-form expression of the performance loss factor is derived as a benchmark. In addition, to take power consumption into account, energy efficiency is also investigated in our paper. The numerical results reveal that the HAD structure with mixed-ADCs can significantly reduce the power consumption and hardware cost. Furthermore, that architecture is able to achieve a better trade-off between the performance loss and the power consumption. Finally, adopting 2-4 bits of resolution may be a good choice in practical massive MIMO systems.

Index Terms—DOA estimation, hybrid analog and digital, mixed-ADC, CRLB, energy efficiency

I. INTRODUCTION

As an important technique in wireless communication, direction of arrival (DOA) estimation has attracted widely attention [1]. DOA estimation has lots of applications, like arrival of angle (AOA) location, sonar, rescue, and tracking of objects. In modern and future communication, DOA estimation may have more potential applications: unmanned aerial vehicle (UAV) communications [5], directional modulation (DM) systems [2]–[4], intelligent reflecting surface (IRS) communications [7]–[9], internet of things (IoT) [6], and millimeter-wave-based massive multiple input multiple output (MIMO) and so on.

It is known that the most methods of DOA estimation are based on spatial spectrum. The multiple signal classification (MUSIC) algorithm was proposed by Schmidt in [10]. However, the MUSIC method needs to obtain a spectrum of all searching angles, which is of high-complexity. Thus,

to refrain from the spectral search in the MUSIC method algorithm, root-MUSIC was proposed in [11], which replaces the spectral search with solving polynomial zeros. In [12], authors proposed another famous search-free method, estimation of signal parameters via rotational invariance technique (ESPRIT). Afterwards, many root-MUSIC-based and ESPRIT-based algorithm were proposed. To improve the performance of the ESPRIT, a total least-squares approach, TLS-ESPRIT, was proposed in [13]. And, authors in [14] proved that the accuracy of the TLS-ESPRIT is close to that of the Cramér-Rao lower bound (CRLB) for fully calibrated sensor arrays. In order to reduce the complexity of the Root-MUSIC, unitary root-MUSIC (U-root-MUSIC) and real-valued root-MUSIC (RV-root-MUSIC) were proposed in [15] and [16], respectively. Recently, more and more concern has been attracted to the DOA estimation for massive MIMO systems. In [17], the DOA estimation in two-dimensional (2-D) massive MIMO systems was investigated with no access to the number of signals, path gain correlations etc. Although the performance of spatial-spectrum-based methods is very satisfactory, the complexity is still high, especially in massive MIMO systems. To deal with that problem, the deep learning is integrated into the DOA estimation for massive MIMO systems in [18]. In [19], the massive MIMO system with one-bit analog-to-digital converters (ADCs) was considered. And, authors proved that the MUSIC algorithm can be applied in the one-bit architecture without modification.

The practical implementation of massive MIMO systems is still difficult. Each antenna is connected to a radio frequency (RF) chain in massive MIMO systems. And, there is an ADC and a digital-to-analog converter (DAC) in every RF chain. It is well-known that the hardware cost and power consumption of ADCs and DACs will increase linearly with the bandwidth and increase exponentially with the number of the quantization bits [20]. Thus, as the number of antennas increases greatly in massive MIMO systems, the power consumption and hardware cost increase rapidly.

To solve this problem, Adopting hybrid analog and digital (HAD) structure is a promising solution. In this structure, Multiple antennas are connected to one RF chain, resulting in the decrease of RF chain number in the antenna array. In recent years, many researchers have focused on the DOA estimation in HAD structure. In [21], four low-complexity and high-resolution algorithm were proposed. And, the exact closed-form expression of the CRLB for HAD structure was derived. To tack the phase-ambiguity in partially-connected

B. Shi and Lingling Zhu are with the School of Electronic and Optical Engineering, Nanjing University of Science and Technology, Nanjing 210094, China.

F. Shu is with the School of Information and Communication Engineering, Hainan University, Haikou 570228, China. (e-mail: shufeng0101@163.com).

Rongen Dong and Qijuan Jie are with the School of Information and Communication Engineering, Hainan University, Haikou 570228, China.

J. Wang is with the School of Engineering and Digital Arts, University of Kent, Canterbury CT2 7NT, U.K. (e-mail: j.z.wang@kent.ac.uk).

HAD structure, authors redesigned the analog phase shifts and estimated the DOA through two steps in [22]. In [23], a 2-D discrete Fourier transform (DFT) based algorithm was proposed. Moreover, authors derived the corresponding CRLB of the channel gain and joint DOA estimation. In [24], authors proposed a beam sweeping algorithm, reconstructing the spatial covariance matrix of the HAD architecture. Then, in [25], a deep-learning-based DOA estimation method for the HAD architecture with a uniform circular array (UCA) was proposed. However, DOA estimation for the HAD architecture with the UCA is still an open problem.

Another promising solution is to substitute the low-resolution ADCs for the high-resolution ADCs. However, the signals quantified by low-resolution ADCs are nonlinear due to the low-precision quantization, which is hard to analyse. In [26], authors presented that using the additive quantization noise model (AQNM) is able to dispel the low-resolution ADCs' distortion. Then, many researches have been focused on the low-resolution structure. Furthermore, authors revealed that, resulting from adopting low-resolution ADCs, the achievable rate will decrease but that can be made up by increasing the number of antennas. Authors investigated the uplink achievable rate for massive MIMO systems when finite resolution ADCs and the common maximal-ratio combining technique were employed at the receive array in [27]. A multipair massive MIMO two-way relay network was considered in [28], where a relay station with a large number of antennas serves multiple pairs of users. In [29], a multipair full-duplex massive MIMO relaying system with low-resolution ADCs at both the relay and receivers was considered. Moreover, authors derived the achievable rates for that case with a finite number of antennas at users. In [30], authors proposed an algorithm for the physical layer security in the massive MIMO system, which was equipped with the analog phase shifters, finite-quantized digital phase shifters and low-resolution ADCs. The performance loss of DOA estimation with low-resolution ADCs was firstly investigated in [31]. In addition, authors discussed the determination of quantization bits. However, a novel DOA estimation method of the low-resolution architecture has not been proposed.

But the low-resolution structure still has some challenges, including time-frequency synchronization, achievable rate and so on [32]–[34]. In order to solve the above problems above, Mixed-ADC architecture, as a new architecture, was proposed to replace the low-resolution structure in [32]. In that structure, some RF chains connect the high-resolution ADCs and the others are connected with the low-resolution ADCs. Thus, more and more scholars have fascinated by the mixed-ADC architecture. In [35], authors investigated the spectral efficiency of massive MIMO systems with mixed-ADCs and proved that the mixed-ADC architecture has a considerable spectral efficiency with a much lower power consumption and circuit cost. The performance of massive MIMO systems with mixed-ADCs over the Rician fading channels was analysed in [33]. The approximate closed-form expressions of the uplink achievable rate for both cases of perfect and imperfect channel state information (CSI) were derived. In [34], authors derived the closed-form expressions of the achievable rate for multipair

massive MIMO relaying systems with mixed-ADCs/DACs. What's more, an efficient power allocation algorithm was proposed. In [36], the performance loss of the DOA estimation for the massive MIMO receive array with mixed-ADCs was investigated. And, authors showed that the mixed-ADC architecture can achieve a good trade-off between the performance loss and power consumption.

In this paper, we consider the DOA estimation in the hybrid analog and digital massive MIMO system with mixed-ADCs. To the best of our knowledge, that case has not been investigated. This study aims to analyse the performance loss and energy efficiency of the DOA estimation for the HAD structure with mixed-ADCs. We show that this new structure can approach the performance of the ideal unquantized system with much lower power consumption. The main contributions of this paper are summarized as follows:

- 1) Considering the nonlinear error caused by the low-resolution ADCs, we build up the system model of the DOA estimation for the HAD architecture with mixed-ADCs by resorting to the AQNM. For the comparison with the conventional full digital structure with pure high-resolution ADCs, we employ the design of analog phase shifters in [21]. Based on that, the root-MUSIC-based method in the HAD structure is proved that it can be used in the HAD architecture with mixed-ADCs without any other modification in the numerical simulation.
- 2) To obtain an accurate performance loss of the DOA estimation for the HAD structure with mixed-ADCs, we define the performance loss factor. Then, we derive the closed-form expression of the CRLB for the HAD structure with mixed-ADCs by the statistic theory and matrix theory. Furthermore, the closed-form expression of the performance loss factor is also derived. Our results show that the HAD structure with mixed-ADCs causes more performance loss than the full digital structure with mixed-ADCs. However, that shortcoming can be made up by increasing the low-resolution ADCs' quantization bits and the number of high-resolution ADCs.
- 3) Finally, in order to assess a thorough investigation on the DOA estimation for the HAD structure with mixed-ADCs, it is essential to study the energy efficiency for that architecture. Combined with the performance loss, the simulation results reveal that although the HAD structure with mixed-ADCs has worse performance, its energy efficiency is much higher. It means that the HAD structure with mixed-ADCs is more suitable for the practical massive MIMO systems. In addition, we find that using 2-4 bits of resolutions can strike a better trade-off and adopting ADCs with longer quantization bits just causes little improvement of performance with much higher power consumption.

The rest of this paper is organized as follows. The system model of the DOA estimation for the HAD structure with mixed-ADCs is presented in Section II. Then, the performance loss and energy efficiency are investigated in Section III. In Section IV, simulation and numerical results are provided to

TABLE I
LINEAR QUANTIZATION GAIN α FOR DIFFERENT QUANTIZATION BITS
($b < 6$)

b	1	2	3	4	5
β	0.3634	0.1175	0.03454	0.009497	0.002499

analyse the performance and trade-off. Finally, we come to the conclusion in Section V.

Notations: In this paper, signs $(\cdot)^T$, $(\cdot)^H$, $|\cdot|$ and $\|\cdot\|$ represent transpose, conjugate transpose, modulus and norm, respectively. \mathbf{x} and \mathbf{X} in bold typeface are used to represent vectors and matrices, respectively, while scalars are presented in normal typeface, such as x . \mathbf{I}_M represents the $M \times M$ identity matrix, $\mathbf{0}_{a \times b}$ denotes the $a \times b$ matrix of all zeros and $\mathbf{1}_M$ denotes the $M \times 1$ vector of all 1. Furthermore, $\mathbb{E}[\cdot]$ and $\Re[\cdot]$ denotes the expectation operator and the real part of a complex-valued number, respectively. \otimes denotes the Kronecker product. $\text{diag}(\mathbf{X})$ denotes a diagonal matrix by keeping only the diagonal elements of matrix \mathbf{X} . $\text{Tr}(\cdot)$ denotes the matrix trace.

II. SYSTEM MODEL

As illustrated in Fig. 1, we consider a sub-connected hybrid analog and digital architecture with mixed-ADCs. A narrow-band signal $s(t)e^{j2\pi f_c t}$ is sent from a far-field emitter and strikes the uniformly-spaced linear array (ULA), where f_c is the carrier frequency. The ULA with M antenna elements is divided into M_s subarrays, and there are M_a antenna elements in the every subarray, $M = M_s M_a$. The propagation delays from the signal to all antenna elements are given by

$$\tau_m = \tau_0 - \frac{d_m}{c} \sin \theta_0, \quad m = 1, 2, \dots, M, \quad (1)$$

where τ_0 , d_m , and c denotes the transmission time from the emitter to the reference point on the array, the distance from the m th antenna element to the reference point, and the speed of the light, respectively. θ_0 represents the direction of arrival, which ranges from -90° to 90° . Thus, the received signal before the analog beamforming (AB) can be expressed as

$$\mathbf{x}(t) = \mathbf{a}(\theta_0)s(t)e^{j2\pi f_c t} + \mathbf{w}(t), \quad (2)$$

where $\mathbf{w}(t)$ denotes the the additive white Gaussian noise (AWGN). Thus, all elements of $\mathbf{w}(t)$ are independent and identically distributed (i.i.d.) and $\mathbf{w}(t) \sim \mathcal{CN}(0, \mathbf{I}_M)$. $\mathbf{a}(\theta_0)$ is the array manifold, which is given by

$$\mathbf{a}(\theta_0) = \left[e^{j\Psi_{\theta_0}(1)} \quad e^{j\Psi_{\theta_0}(2)} \quad \dots \quad e^{j\Psi_{\theta_0}(M)} \right]^T, \quad (3)$$

where

$$\Psi_{\theta_0}(m) = 2\pi \sin \theta_0 \frac{d_m}{\lambda}, \quad m = 1, 2, \dots, M, \quad (4)$$

is the signal phases of m th antenna element, corresponding to the propagation delay difference between m th antennal element and the reference point. Hence, for the ULA, if we choose the endpoint element as the reference point, d_m is given by

$$d_m = (m-1)d, \quad m = 1, 2, \dots, M, \quad (5)$$

where d is the antenna spacing. Furthermore, d_m can be written as

$$d_{m_s, m_a} = [(m_s - 1)M_a + m_a - 1]d, \\ m_s = 1, 2, \dots, M_s, \quad m_a = 1, 2, \dots, M_a. \quad (6)$$

After going through the AB and RF chain, the signal is down-converted from frequency band to baseband, which is given by

$$\mathbf{y}(t) = \mathbf{V}_A^H \mathbf{a}(\theta_0)s(t) + \mathbf{w}(t), \quad (7)$$

where the AB matrix is defined by

$$\mathbf{V}_A = \begin{bmatrix} \mathbf{v}_{A,1} & \mathbf{0} & \dots & \mathbf{0} \\ \mathbf{0} & \mathbf{v}_{A,2} & \dots & \mathbf{0} \\ \vdots & \vdots & \ddots & \vdots \\ \mathbf{0} & \mathbf{0} & \dots & \mathbf{v}_{A,M_s} \end{bmatrix}, \quad (8)$$

where

$$\mathbf{v}_{A, m_s} = \frac{1}{\sqrt{M_a}} \left[e^{j\omega_{m_s,1}} \quad e^{j\omega_{m_s,2}} \quad \dots \quad e^{j\omega_{m_s, M_a}} \right]^T \quad (9)$$

is the AB vector of the m_s th subarray.

Different from the conventional HAD structure with pure high-resolution ADCs, M_0 RF chains are connected with high-resolution ADCs and the other M_1 RF chains are connected with low-resolution ADCs in our architecture, which means $M_s = M_0 + M_1$. Then, $\kappa \triangleq M_0/M_s$ ($0 \leq \kappa \leq 1$) is defined as the proportion of the high-resolution ADCs. Thus, $\mathbf{y}(t)$ can be divided into two parts as (10), shown at the bottom of this page. The received signals passing through high-resolution ADCs can be given by

$$\mathbf{y}_0(n) = \mathbf{y}_0(t)|_{t=n} = \mathbf{V}_{A,0}^H \mathbf{a}_0(\theta_0)s(n) + \mathbf{w}_0(n) \\ n = 1, 2, \dots, N \quad (11)$$

where N is the number of snapshots, and $\mathbf{w}_0(n) \sim \mathcal{CN}(\mathbf{0}, \mathbf{I}_{M_0})$ denotes the AWGN vector with i.i.d. components following the distribution $\mathcal{CN}(0, 1)$. By resorting to the additive quantization noise model (AQNM) widely adopted in massive MIMO systems [33], [37], [38], the nonlinear quantization error caused by the low-resolution ADCs can be transmitted into a linear gain with the additional noise.

$$\mathbf{y}_1(n) = \mathbb{Q}\{\mathbf{y}_1(t)\} = \alpha \mathbf{V}_{A,1}^H \mathbf{a}_1(\theta_0)s(n) + \alpha \mathbf{w}_1(n) + \mathbf{w}_q(n) \\ n = 1, 2, \dots, N \quad (12)$$

$$\mathbf{y}(t) = \begin{bmatrix} \mathbf{y}_0(t) \\ \mathbf{y}_1(t) \end{bmatrix} = \begin{bmatrix} \mathbf{V}_{A,0} & \mathbf{0}_{M_0 \times M_1} \\ \mathbf{0}_{M_1 \times M_0} & \mathbf{V}_{A,1} \end{bmatrix} \begin{bmatrix} \mathbf{a}_0(\theta_0) \\ \mathbf{a}_1(\theta_0) \end{bmatrix} s(t) + \begin{bmatrix} \mathbf{w}_0(t) \\ \mathbf{w}_1(t) \end{bmatrix} \quad (10)$$

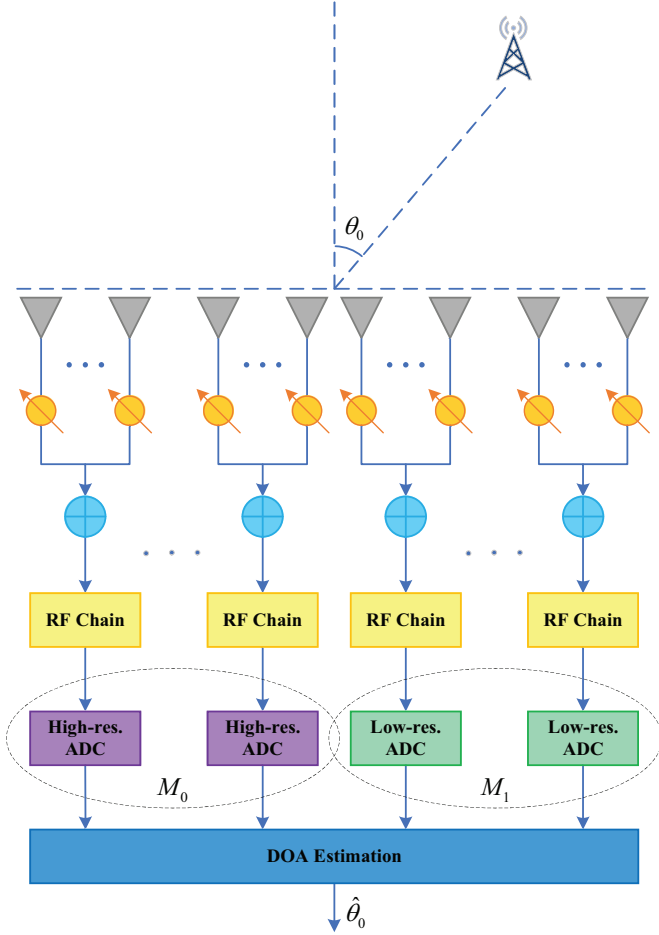


Fig. 1. System model of the HAD architecture with mixed-ADCs

where $\mathbf{w}_1(n) \sim \mathcal{CN}(0, \mathbf{I}_{M_1})$, $\mathbb{Q}\{\cdot\}$ is the quantization function of the low-resolution ADCs, $\mathbf{w}_q(n)$ is the quantization noise related to the $\mathbf{y}_1(t)$, and $\alpha = 1 - \beta$ is a linear gain, where β denotes the distortion factor of the low-resolution ADCs, defined by

$$\beta = \frac{\mathbb{E}[\|\mathbf{y} - \mathbf{y}_q\|^2]}{\mathbb{E}[\|\mathbf{y}\|^2]}. \quad (13)$$

The exact values of β with different quantization bits are listed in Table I. When $b > 5$, the distortion factor β can be approximated as

$$\beta \approx \frac{\sqrt{3}\pi}{2} \cdot 2^{-2b}, \quad b \geq 6. \quad (14)$$

Then, the covariance matrix of $\mathbf{w}_q(n)$ can be expressed as

$$\mathbf{R}_{\mathbf{w}_q} = \alpha\beta \mathbf{diag}(\sigma_s^2 \mathbf{V}_{A,1}^H \mathbf{a}_1(\theta) \mathbf{a}_1^H(\theta) \mathbf{V}_{A,1} + \mathbf{I}_{M_1}). \quad (15)$$

By combining (11) and (12), the total quantized signal is given by

$$\mathbf{y}(n) = \begin{bmatrix} \mathbf{y}_0(n) \\ \mathbf{y}_1(n) \end{bmatrix} \approx \begin{bmatrix} \mathbf{V}_{A,0} \mathbf{a}_0(\theta) \mathbf{s}(n) + \mathbf{w}_0(n) \\ \alpha \mathbf{V}_{A,1} \mathbf{a}_1(\theta) \mathbf{s}(n) + \alpha \mathbf{w}_1(n) + \mathbf{w}_q(n) \end{bmatrix}. \quad (16)$$

III. PERFORMANCE ANALYSIS

In this section, the performance loss and energy efficiency is analyzed for the HAD structure with mixed-ADCs.

A. Performance Loss

In this subsection, to obtain the accurate performance loss, we derive the the closed-form expressions of the CRLB in this architecture. By utilizing the Root-MUSIC-HDAPA DOA method in [21] as a benchmark, we prove that the existing methods of the DOA estimation in HAD structure can be used without other modification and evaluate the practical performance of proposed architecture.

Consider the low-complexity and high-resolution method in [21], where the analog beamforming is set as $\mathbf{v}_{A,m_s} = \frac{1}{\sqrt{M_a}} [1 \ 1 \ \dots \ 1]^T$, $m_s = 1, 2, \dots, M_s$. Thus, the covariance matrix of quantization noise can be given by

$$\begin{aligned} \mathbf{R}_{\mathbf{w}_q} &= \alpha\beta \mathbf{diag}(\sigma_s^2 \mathbf{V}_{A,1}^H \mathbf{a}_1(\theta) \mathbf{a}_1^H(\theta) \mathbf{V}_{A,1} + \mathbf{I}_{M_1}) \\ &= \alpha\beta \mathbf{diag} \left(\frac{\sigma_s^2 \|\zeta\|^2}{M_a} \mathbf{a}_{s,1}(\theta) \mathbf{a}_{s,1}^H(\theta) + \mathbf{I}_{M_1} \right) \\ &= \alpha\beta \left(\frac{\gamma \|\zeta\|^2}{M_a} + 1 \right) \mathbf{I}_{M_1}, \end{aligned} \quad (17)$$

where $\gamma = \sigma_s^2 / \sigma_n^2 = \sigma_s^2$ is the input SNR of the received signal,

$$\begin{aligned} \mathbf{a}_{s,1}(\theta) &= e^{j \frac{2\pi}{\lambda} M_0 d \sin \theta_0} \\ &\times \left[1 \ e^{j \frac{2\pi}{\lambda} M_a d \sin \theta_0} \ \dots \ e^{j \frac{2\pi}{\lambda} (M_1 - 1) M_a d \sin \theta_0} \right]^T, \end{aligned} \quad (18)$$

and

$$\zeta = \sum_{m_a=1}^{M_a} e^{j \frac{2\pi}{\lambda} d_{1,m_a} \sin \theta_0} = \frac{1 - e^{j \frac{2\pi}{\lambda} M_a d \sin \theta_0}}{1 - e^{j \frac{2\pi}{\lambda} d \sin \theta_0}}. \quad (19)$$

Therefore, we have $\mathbf{w}_q \sim \mathcal{CN}(0, \sigma_q^2 \mathbf{I}_{M_1})$, where $\sigma_q^2 = \alpha\beta \left(\frac{\gamma \|\zeta\|^2}{M_a} + 1 \right)$. And, the FIM for the hybrid structure with mixed-ADCs is calculated in the Appendix, which is given as (20), shown at the bottom of the last page. Due to

$$\mathbf{CRLB} = \frac{1}{N} \mathbf{F}^{-1}, \quad (21)$$

the CRLB of the direction can be expressed as

$$\text{var}(\hat{\theta}_0) \geq \frac{\lambda^2 M_a (\gamma \|\zeta\|^2 + M_a)^2}{8\varphi N \pi^2 \gamma^2 \cos^2 \theta_0}, \quad (22)$$

where

$$\begin{aligned} \varphi &= \|\zeta\|^4 (\xi \nu - \mu^2) (\gamma \|\zeta\|^2 + M_a) \\ &+ M_a \xi^2 \left(\|\zeta\|^2 \|\Gamma\|^2 - \Re \left[(\Gamma^H \zeta)^2 \right] \right). \end{aligned} \quad (23)$$

Referring to [31], we define the performance loss factor as

$$\eta_{PL} = \frac{\mathbf{CRLB}_{\theta_0}}{\mathbf{CRLB}_{\theta_0}^{M_a=1, \kappa=1}}. \quad (24)$$

From (22), the performance loss factor can be given as (25). Different from the performance loss factor in [36], $M_a/M = 1/M_s \approx 0$ is invalid in HAD structure, especially when γ is low and M_a is high. Thus, the impact of the M on the performance loss is hard to be ignored in our architecture.

B. Energy Efficiency

Although we have investigated the performance loss, it is hard to assess the the HAD structure with mixed-ADCs if we only consider the performance loss. Therefore, to achieve a better trade-off, it is obliged to discussed the power consumption of the HAD structure with mixed-ADCs. Due to this reason, the power consumption and energy efficiency for the DOA estimation is studied in the HAD structure with mixed-ADCs.

According to [36], the energy efficiency factor can be defined as

$$\eta_{EE} = \frac{CRLB_{\theta_0}^{-\frac{1}{2}}}{P_t} \text{ 1/degree/W}, \quad (26)$$

where P_t is the total power consumption in the system [34], which can be given by

$$P_t = MP_{APS} + P_{RF} + M_0(P_{AGC} + P_{HADC}) + M_1(\chi P_{AGC} + P_{LADC}) \quad (27)$$

where P_{APS} , P_{RF} , P_{AGC} , P_{HADC} and P_{LADC} denotes the the power consumption of the analog phase shifter, the RF chain, the automatic gain control (AGC), the high-resolution ADC and the low-resolution ADC, respectively. Among them,

$$P_{RF} = M_s(P_{LNA} + P_m + P_f + P_{IFA}) + P_{fsyc} \quad (28)$$

where P_{LNA} , P_m , P_f , P_{IFA} and P_{fsyc} represent the power consumption of the low-noise amplifiers (LNA), the mixer, the filter, the intermediate frequency amplifier (IFA) and the frequency synthesizer, respectively. Besides, χ is a flag function connected with the number of the ADCs' quantization bit, which is given by

$$\chi = \begin{cases} 0, & b = 1, \\ 1, & b > 1. \end{cases} \quad (29)$$

Furthermore, by consulting [39], P_{ADC} can be expressed as

$$P_{ADC} \approx \frac{3V_{dd}^2 L_{min}(f_{cor} + 2B)}{10^{-0.1525b+4.838}}. \quad (30)$$

where V_{dd} is the power supply of converter, B is the bandwidth of received signal, f_{cor} is the corner frequency of the 1/f noise [39], and L_{min} denotes the the minimum channel length for the given CMOS technology. It is difficult to analyse the (26). Thus, detailed results are presented in Section IV.

$$\mathbf{F} = \begin{bmatrix} \left(\frac{\xi \|\zeta\|^2}{\gamma \xi \|\zeta\|^2 + M_a} \right)^2 & 0 \\ 0 & \frac{8\pi^2 \gamma^2 \cos^2 \theta_0}{\lambda^2 M_a (\gamma \xi \|\zeta\|^2 + M_a)^2} \left[\|\zeta\|^4 (\xi \nu - \mu^2) (\gamma \xi \|\zeta\|^2 + M_a) + M_a \xi^2 \left(\|\zeta\|^2 \|\Gamma\|^2 - \mathbb{R} \left[(\Gamma^H \zeta)^2 \right] \right) \right] \end{bmatrix} \quad (20)$$

$$\eta_{PL} = \frac{M^2 d^2 (M^2 - 1) (\gamma \xi \|\zeta\|^2 + M_a)^2}{12(\gamma M + 1) \left[\|\zeta\|^4 (\xi \nu - \mu^2) (\gamma \xi \|\zeta\|^2 + M_a) + M_a \xi^2 \left(\|\zeta\|^2 \|\Gamma\|^2 - \mathbb{R} \left[(\Gamma^H \zeta)^2 \right] \right) \right]}. \quad (25)$$

IV. SIMULATION AND DISCUSSION

In this section, simulation results are presented to verify the the accuracy of the analytical results. Then, the curves of performance loss for different conditions are shown. Then, the root-MUSIC-based algorithm in the HAD architecture is demonstrated to show the practical performance of this architecture. Moreover, the energy efficiency is investigated to present the advantage of the HAD architecture with mixed-ADCs and provide the suggestions of choices for quantization bits.

In the simulations, we assume that the parameters are chosen as follow: $\theta_0 = 15^\circ$, $N = 32$, $\kappa = 1/4$ and $M = 128$. To assess the performance of the methods in practical, the root mean square error (RMSE) is adopted in simulations, which is given by

$$RMSE = \sqrt{\frac{1}{N_t} \sum_{n_t=1}^{N_t} (\hat{\theta}_{n_t} - \theta_0)^2}, \quad (31)$$

where N_t is the number of numerical simulations, which is set as 18000.

The impact of the SNR on the performance loss is shown in Fig. 2. Three cases are investigated: (a) $\kappa = 0$ (equipped with pure low-resolution ADCs), (b) $\kappa = 1/4$ (equipped with little high-resolution ADCs), (c) $\kappa = 3/4$ (equipped with many high-resolution ADCs). In each case, the full digital structure with mixed-ADCs ($M_a = 1$) is plotted for comparison. It is worth noting that curves of $M_a = 4$ are all higher than those of $M_a = 1$ and all curves increase as the SNR increases. An insightful observation is that the HAD structure causes more performance loss, which is about 5dB when $M_a = 4$. Moreover, as the SNR increases, the performance loss increases rapidly. Thus, we should choose larger quantization bits of low-resolution ADCs at high SNR. However, as κ increases, that trend slows down, which means the performance loss decreases as κ increases. Therefore, adopting more high-resolution ADCs is another option at high SNR.

Fig. 3 illustrates the performance loss versus the quantization bits for different M_a . It is clear that the performance loss decreases as the quantization bits increase for all cases. And, the performance loss is bigger at higher SNR, which is consistent with Fig. 2. We also find that increasing the quantization bits has negligible performance improvement when $b > 5$. It is seen from Fig. 3 that the performance loss for $\gamma = -10dB$ is worse than other cases as the quantization bits

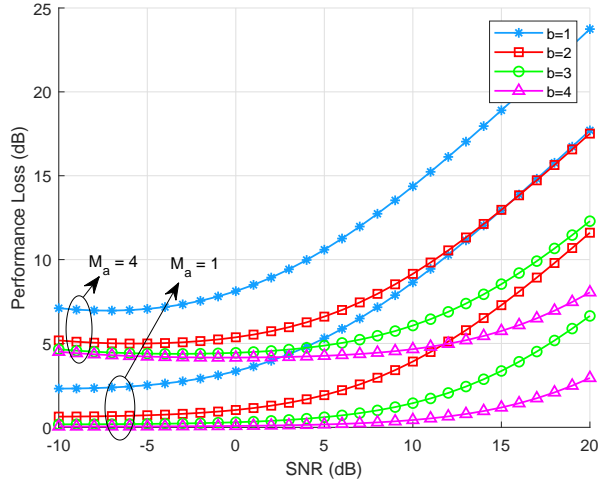
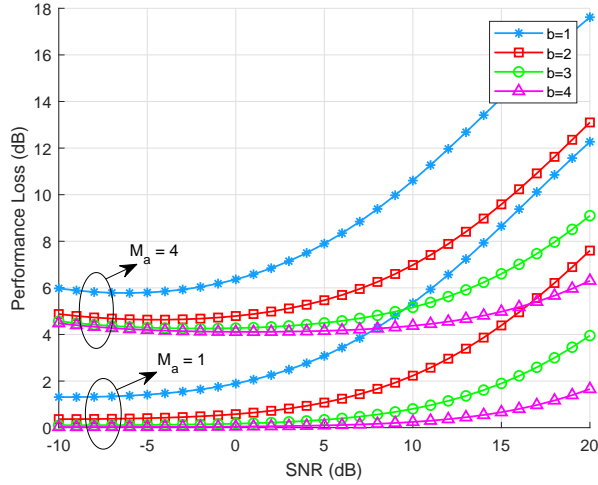
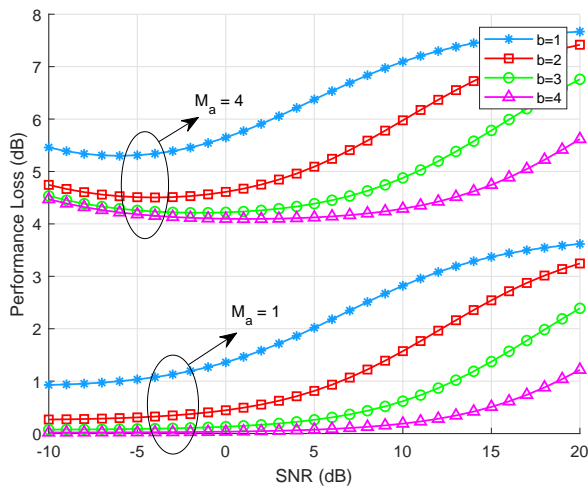
(a) $\kappa = 0$ (b) $\kappa = 1/4$ (c) $\kappa = 3/4$

Fig. 2. Comparison of the performance loss for the DOA estimation versus the SNR with the different κ .

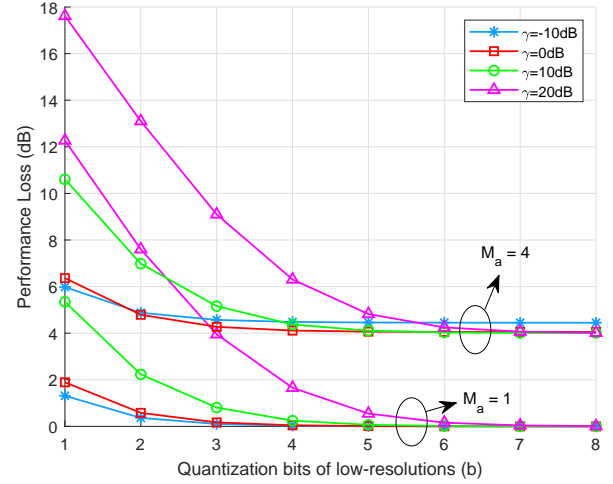


Fig. 3. Performance loss over quantization bits of low-resolution ADCs.

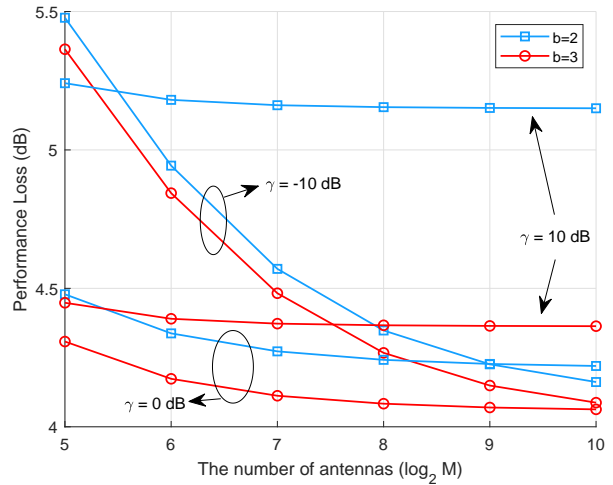


Fig. 4. Performance loss over the number of antennas with different quantization bits and SNR.

increase when $M_a = 4$. Furthermore, the similar loss is seen at very low SNR in Fig. 2(c). That loss is caused by the nature of the HAD structure. Thus, the HAD structure with mixed-ADCs has the best performance about 0dB. In conclusion, just 2-3 bits of the resolution can causes little performance loss. In addition, at the high SNR, adopting 4-5 bits' ADCs is a better choice. However, bigger quantization bits is not recommended.

In Fig. 4, the performance loss for the HAD architecture with mixed-ADCs against the number of antennas is plotted. The number of antennas M ranges from 32 to 1024. And, the quantization bits of two different values, $b = 2, 3$, are considered. It can be seen that all curves decrease as the number of antennas increases. However, as the SNR increases, the slope of the corresponding curves becomes smaller. Especially, the curves are almost flat when $\gamma = 10dB$. An insightful observation is that the HAD structure with mixed-ADCs is very suitable to many future practical application scenarios because the number of antennas in the massive MIMO system

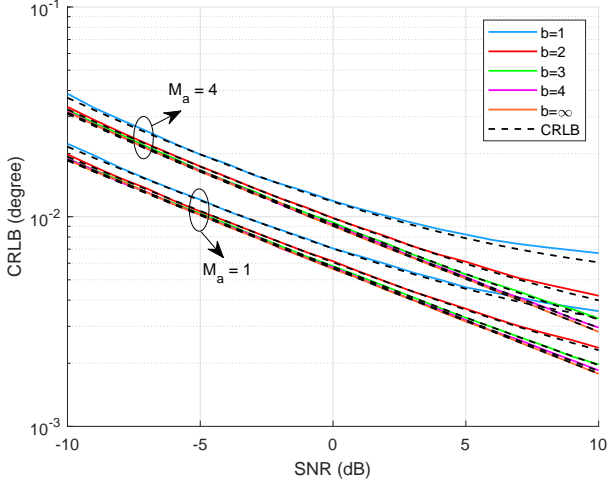


Fig. 5. RMSE versus SNR for $M_a = 1$ and $M_a = 4$

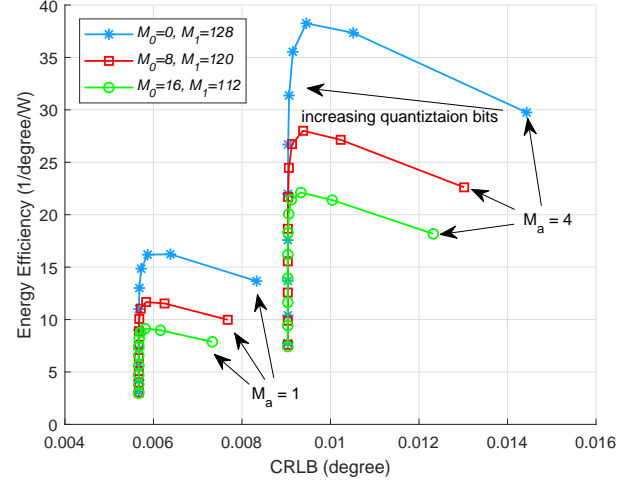


Fig. 7. Trade-off between the CRLB and the energy efficiency

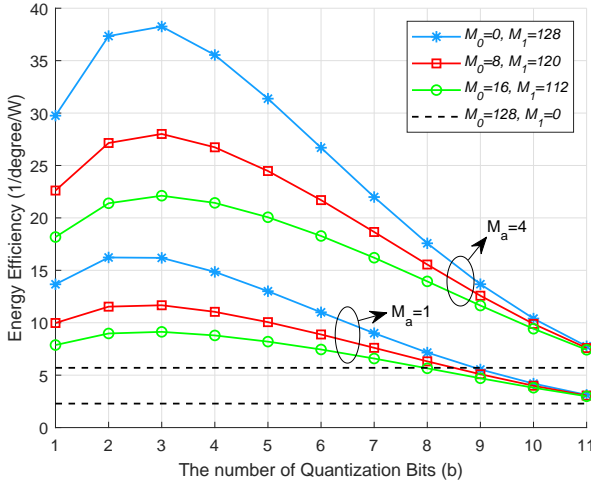


Fig. 6. Energy efficiency of the HAD architecture with mixed-ADCs against different quantization bits

is going to increase bigger and bigger and the SNR in many DOA estimation scenarios is low.

The RMSE of the DOA estimation versus SNR with $\kappa = 1/4$ for different quantization bits and the number of antennas in the each subarray is presented in Fig. 5. The SNR ranges from -10dB to 10dB. The curves of full digital structure is illustrated, too. The first insight obtained from Fig. 5 is that the root-MUSIC-based algorithm in the HAD structure in [21] can achieve the corresponding CRLB. And, the RMSE of the HAD structure with mixed-ADCs is higher than that of the full digital structure with mixed-ADCs. In addition, similar to Fig. 2, the gaps of different quantization bits become large when the SNR increases. Finally, adopting 3-4 bits of resolutions can result in negligible performance loss at high SNR.

In Fig. 6, the energy efficiency for the HAD architecture with mixed-ADCs versus the ADCs' quantization bits is shown. Herein, three different cases are considered as

follow: 1) $M_0 = 0, M_1 = 128$, 2) $M_0 = 8, M_1 = 120$, 3) $M_0 = 16, M_1 = 112$. In our simulation, the values in massive MIMO systems are chosen as follow: $P_{APSS} = 1$ mW, $P_{LNA} = 20$ mW, $P_{mix} = 30.3$ mW, $P_{fil} = 2.5$ mW, $P_{IFA} = 3$ mW, $P_{sync} = 50.5$ mW, $P_{AGC} = 2$ mW, $V_{dd} = 3$ V, $B = 20$ MHz, $L_{min} = 0.5$ μ m and $f_{cor} = 1$ MHz as in [34], [40], [41]. And, 12 is adopted as the number of quantization bit for high-resolution ADCs. As can be seen, all curves have peaks and the positions of peaks. And, compared with curves with $M_a = 1$, the positions of peaks moves to right for the curves with $M_a = 4$. This important finding demonstrates that compared with the full digital structure with mixed-ADCs, the HAD structure with mixed-ADCs has much higher energy efficiency. In addition, the energy efficiency decreases as the proportion of the high-resolution ADCs increases. Thus, the array with pure high-resolution ADCs has lowest energy efficiency, which implies that adopting low-resolution ADCs is effective. In summary, the HAD architecture with mixed-ADCs is superior to the HAD architecture and the mixed-ADC structure, which has higher energy efficiency.

In Fig. 7, we show the trade-off between the CRLB and energy efficiency with different proportions of the high-resolution ADCs. The curves of the full digital structure with mixed-ADCs ($M_a = 1$) are also plotted as a benchmark. It is seen that the HAD structure with mixed-ADCs has much higher energy efficiency. And, adopting pure low-resolution ADCs can achieve the best energy efficiency. However, considering the poor performance of DOA estimation in Fig. 2 and low achievable rate in [33], it is hard to employ the pure low-resolution ADCs structure in the practical massive MIMO systems. Moreover, we can conclude that the energy efficiency increases as the proportion of the high-resolution ADCs, κ , decreases. When we increase the number of quantization bits from 1 to 4, the CRLB will decrease quickly. While the performance almost has no improvement when quantization bits range from 4 to 12 bits. In addition, increasing ADCs' resolution in the HAD structure has more performance improvement than that in the full digital structure.

V. CONCLUSION

In this paper, the performance of the DOA estimation for the hybrid analog and digital structure with mixed-ADCs in massive MIMO systems has been investigated. We have established the system model of the DOA estimation for the HAD massive MIMO system with mixed-ADCs. Then, the performance loss factor has been defined for that architecture. Furthermore, the closed-form expression of the corresponding CRLB has been derived. Based on that, the closed-form expression of performance loss factor has been also derived. In addition, we have studied the energy efficiency for that architecture and found that adopting 2-4 quantization bit for the low-resolution ADCs can obtain a better trade-off. Finally, we can draw the conclusion that the HAD structure with mixed-ADCs can obtain a much lower power consumption and radio frequency cost with little performance loss.

APPENDIX

DERIVATION OF THE FIM FOR THE HAD ARCHITECTURE WITH MIXED-ADCs

In this section, to have access to the Cramér-Rao lower bound (CRLB) for hybrid structure with mixed-ADCs, we derive the closed-form expression for the corresponding Fisher information matrix (FIM). Considering the θ_0 and γ are all unknown, \mathbf{F} can be divided as

$$\mathbf{F} = \begin{bmatrix} \mathbf{F}_{\gamma,\gamma} & \mathbf{F}_{\gamma,\theta_0} \\ \mathbf{F}_{\gamma,\theta_0} & \mathbf{F}_{\theta_0,\theta_0} \end{bmatrix}. \quad (32)$$

In accordance with [1], the elements of \mathbf{F} can be calculated by

$$\mathbf{F}_{\gamma,\gamma} = \text{Tr} \left\{ \mathbf{R}_y^{-1} \frac{\partial \mathbf{R}_y}{\partial \gamma} \mathbf{R}_y^{-1} \frac{\partial \mathbf{R}_y}{\partial \gamma} \right\}, \quad (33)$$

$$\mathbf{F}_{\gamma,\theta_0} = \text{Tr} \left\{ \mathbf{R}_y^{-1} \frac{\partial \mathbf{R}_y}{\partial \gamma} \mathbf{R}_y^{-1} \frac{\partial \mathbf{R}_y}{\partial \theta_0} \right\}, \quad (34)$$

$$\mathbf{F}_{\theta_0,\gamma} = \text{Tr} \left\{ \mathbf{R}_y^{-1} \frac{\partial \mathbf{R}_y}{\partial \theta_0} \mathbf{R}_y^{-1} \frac{\partial \mathbf{R}_y}{\partial \gamma} \right\}, \quad (35)$$

and

$$\mathbf{F}_{\theta_0,\theta_0} = \text{Tr} \left\{ \mathbf{R}_y^{-1} \frac{\partial \mathbf{R}_y}{\partial \theta_0} \mathbf{R}_y^{-1} \frac{\partial \mathbf{R}_y}{\partial \theta_0} \right\}. \quad (36)$$

Firstly, let us abbreviate $s(n)$, $\mathbf{y}(n)$, $\mathbf{a}(\theta_0)$ and $\mathbf{w}(n)$ as s , \mathbf{y} , \mathbf{a} and \mathbf{w} , respectively. Then, \mathbf{y} can be rewritten as

$$\mathbf{y} = \mathbf{T} \mathbf{V}_A^H \mathbf{a} \mathbf{s} + \mathbf{T} \mathbf{w} + \mathbf{q}, \quad (37)$$

where

$$\mathbf{T} = \begin{bmatrix} \mathbf{I}_{M_0} & \mathbf{0}_{M_0 \times M_1} \\ \mathbf{0}_{M_1 \times M_0} & \alpha \mathbf{I}_{M_1} \end{bmatrix} \quad (38)$$

and

$$\mathbf{q} = \begin{bmatrix} \mathbf{0}_{M_0 \times 1} \\ \mathbf{w}_q \end{bmatrix}. \quad (39)$$

Thus, the covariance matrix of \mathbf{y} is derived by

$$\mathbf{R}_y = \mathbb{E}[\mathbf{y} \mathbf{y}^H] = \gamma \mathbf{T} \mathbf{V}_A^H \mathbf{a} \mathbf{a}^H \mathbf{V}_A \mathbf{T}^H + \mathbf{Q}, \quad (40)$$

where

$$\begin{aligned} \mathbf{Q} &= \mathbb{E}[\mathbf{T} \mathbf{w} \mathbf{w}^H \mathbf{T}^H + \mathbf{q} \mathbf{q}^H] \\ &= \begin{bmatrix} \mathbf{I}_{M_0} & \mathbf{0}_{M_0 \times M_1} \\ \mathbf{0}_{M_1 \times M_0} & (\alpha^2 + \sigma_q^2) \mathbf{I}_{M_1} \end{bmatrix}. \end{aligned} \quad (41)$$

where $\sigma_q^2 = \alpha \beta \left(\frac{\gamma \|\xi\|^2}{M_a} + 1 \right)$ is defined in (17). Accordingly, the partial derivatives of \mathbf{R}_y are given by

$$\frac{\partial \mathbf{R}_y}{\partial \gamma} = \mathbf{T} \mathbf{V}_A^H \mathbf{a} \mathbf{a}^H \mathbf{V}_A \mathbf{T}^H \quad (42)$$

and

$$\frac{\partial \mathbf{R}_y}{\partial \theta_0} = \gamma \mathbf{T} \mathbf{V}_A^H (\mathbf{a}' \mathbf{a}^H + \mathbf{a} \mathbf{a}'^H) \mathbf{V}_A \mathbf{T}^H. \quad (43)$$

where \mathbf{a}' is the derivative for the array manifold to θ_0 , which is given by

$$\mathbf{a}' = \frac{d}{d\theta_0} \mathbf{a}(\theta_0) = j \frac{2\pi}{\lambda} \cos \theta_0 \mathbf{D} \mathbf{a} \quad (44)$$

where

$$\mathbf{D} = \begin{bmatrix} d_1 & 0 & \cdots & 0 \\ 0 & d_2 & \cdots & 0 \\ \vdots & \vdots & \ddots & \vdots \\ 0 & 0 & \cdots & d_M \end{bmatrix}. \quad (45)$$

By utilizing the well-known Sherman-Morrison matrix identity in [42],

$$(\mathbf{A} + \mathbf{BCD})^{-1} = \mathbf{A}^{-1} - \mathbf{A}^{-1} \mathbf{B} (\mathbf{C}^{-1} + \mathbf{D} \mathbf{A}^{-1} \mathbf{B})^{-1} \mathbf{D} \mathbf{A}^{-1}, \quad (46)$$

we can obtain

$$\mathbf{R}_y^{-1} = \mathbf{Q}^{-1} - \frac{\mathbf{Q}^{-1} \mathbf{T} \mathbf{V}_A^H \mathbf{a} \mathbf{a}^H \mathbf{V}_A \mathbf{T}^H \mathbf{Q}^{-1}}{\gamma^{-1} + \mathbf{a}^H \mathbf{V}_A \mathbf{T}^H \mathbf{Q}^{-1} \mathbf{T} \mathbf{V}_A^H \mathbf{a}}. \quad (47)$$

Let us derive the $\mathbf{F}_{\gamma,\gamma}$ firstly, which can be expanded to

$$\begin{aligned} \mathbf{F}_{\gamma,\gamma} &= \text{Tr} \left\{ \mathbf{R}_y^{-1} \mathbf{T} \mathbf{V}_A^H \mathbf{a} \mathbf{a}^H \mathbf{V}_A \mathbf{T}^H \mathbf{R}_y^{-1} \mathbf{T} \mathbf{V}_A^H \mathbf{a} \mathbf{a}^H \mathbf{V}_A \mathbf{T}^H \right\} \\ &= \left[\mathbf{a}^H \mathbf{V}_A \mathbf{T}^H \left(\mathbf{Q}^{-1} \right. \right. \\ &\quad \left. \left. - \frac{\mathbf{Q}^{-1} \mathbf{T} \mathbf{V}_A^H \mathbf{a} \mathbf{a}^H \mathbf{V}_A \mathbf{T}^H \mathbf{Q}^{-1}}{\gamma^{-1} + \mathbf{a}^H \mathbf{V}_A \mathbf{T}^H \mathbf{Q}^{-1} \mathbf{T} \mathbf{V}_A^H \mathbf{a}} \right) \mathbf{T} \mathbf{V}_A^H \mathbf{a} \right]^2 \\ &= \left[\mathbf{a}^H \mathbf{B} \mathbf{a} - \frac{(\mathbf{a}^H \mathbf{B} \mathbf{a})^2}{\gamma^{-1} + \mathbf{a}^H \mathbf{B} \mathbf{a}} \right]^2, \end{aligned} \quad (48)$$

$$\begin{aligned} \mathbf{F}_{\theta_0,\theta_0} &= \gamma^2 \text{Tr} \left\{ \mathbf{R}_y^{-1} \mathbf{T} \mathbf{V}_A^H (\dot{\mathbf{a}} \mathbf{a}^H + \mathbf{a} \dot{\mathbf{a}}^H) \mathbf{V}_A \mathbf{T}^H \mathbf{R}_y^{-1} \mathbf{T} \mathbf{V}_A^H (\dot{\mathbf{a}} \mathbf{a}^H + \mathbf{a} \dot{\mathbf{a}}^H) \mathbf{V}_A \mathbf{T}^H \right\} \\ &= \gamma^2 \left[(\mathbf{a}^H \mathbf{V}_A \mathbf{T}^H \mathbf{R}_y^{-1} \mathbf{T} \mathbf{V}_A^H \dot{\mathbf{a}})^2 + 2(\mathbf{a}^H \mathbf{V}_A \mathbf{T}^H \mathbf{R}_y^{-1} \mathbf{T} \mathbf{V}_A^H \mathbf{a})(\dot{\mathbf{a}}^H \mathbf{V}_A \mathbf{T}^H \mathbf{R}_y^{-1} \mathbf{T} \mathbf{V}_A^H \dot{\mathbf{a}}) + (\dot{\mathbf{a}}^H \mathbf{V}_A \mathbf{T}^H \mathbf{R}_y^{-1} \mathbf{T} \mathbf{V}_A^H \mathbf{a})^2 \right] \\ &= \gamma^2 (F_a + 2F_b + F_c) \end{aligned} \quad (63)$$

where

$$\mathbf{B} = \mathbf{V}_A \mathbf{T}^H \mathbf{Q}^{-1} \mathbf{T} \mathbf{V}_A^H. \quad (49)$$

By resorting to the Kronecker product, we have

$$\mathbf{B} = \frac{1}{M_a} \mathbf{C} \otimes (\mathbf{1}_{M_a} \mathbf{1}_{M_a}^H), \quad (50)$$

where

$$\mathbf{C} = \begin{bmatrix} \mathbf{I}_{M_0} & \mathbf{0}_{M_0 \times M_1} \\ \mathbf{0}_{M_1 \times M_0} & \frac{\alpha^2}{\alpha^2 + \sigma_q^2} \mathbf{I}_{M_1} \end{bmatrix}, \quad (51)$$

and

$$\mathbf{a} = \mathbf{a}_s \otimes \mathbf{a}_a, \quad (52)$$

where

$$\mathbf{a}_s = [1, e^{j\frac{2\pi}{\lambda} M_a d \sin \theta_0}, \dots, e^{j\frac{2\pi}{\lambda} (M_s-1) M_a d \sin \theta_0}]^T, \quad (53)$$

and

$$\mathbf{a}_a = [1, e^{j\frac{2\pi}{\lambda} d \sin \theta_0}, \dots, e^{j\frac{2\pi}{\lambda} (M_a-1) d \sin \theta_0}]^T. \quad (54)$$

Hence, referring to the properties of Kronecker product in [42],

$$(\mathbf{A} \otimes \mathbf{B})(\mathbf{C} \otimes \mathbf{D}) = \mathbf{AC} \otimes \mathbf{BD} \quad (55a)$$

$$\mathbf{Tr}(\mathbf{X} \otimes \mathbf{Y}) = \mathbf{Tr}(\mathbf{X})\mathbf{Tr}(\mathbf{Y}), \quad (55b)$$

we have

$$\begin{aligned} \mathbf{a}^H \mathbf{B} \mathbf{a} &= \frac{1}{M_a} (\mathbf{a}_s \otimes \mathbf{a}_a)^H (\mathbf{C} \otimes \mathbf{1}_{M_a} \mathbf{1}_{M_a}^H) (\mathbf{a}_s \otimes \mathbf{a}_a) \\ &= \frac{1}{M_a} (\mathbf{a}_s^H \mathbf{C} \mathbf{a}_s \otimes \mathbf{a}_a^H \mathbf{1}_{M_a} \mathbf{1}_{M_a}^H \mathbf{a}_a) \\ &= \frac{1}{M_a} \left(M_0 + \frac{\alpha^2}{\alpha^2 + \sigma_q^2} M_1 \right) \|\mathbf{1}_{M_a}^H \mathbf{a}_a\|^2 \\ &= \frac{1}{M_a} \xi \|\zeta\|^2, \end{aligned} \quad (56)$$

where

$$\xi = M_0 + \frac{\alpha^2}{\alpha^2 + \sigma_q^2} M_1. \quad (57)$$

Thus, $\mathbf{F}_{\gamma, \gamma}$ can be expressed as

$$\mathbf{F}_{\gamma, \gamma} = \left(\frac{\xi \|\zeta\|^2}{\gamma \xi \|\zeta\|^2 + M_a} \right)^2. \quad (58)$$

Similarly, $\mathbf{F}_{\gamma, \theta_0}$ can be given by

$$\begin{aligned} \mathbf{F}_{\gamma, \theta_0} &= \gamma \mathbf{Tr} \left\{ \mathbf{R}_y^{-1} \mathbf{T} \mathbf{V}_A^H \mathbf{a} \mathbf{a}^H \mathbf{V}_A \mathbf{T}^H \mathbf{R}_y^{-1} \mathbf{T} \mathbf{V}_A^H (\mathbf{a}' \mathbf{a}^H \right. \\ &\quad \left. + \mathbf{a} \mathbf{a}^H) \mathbf{V}_A \mathbf{T}^H \right\} \\ &= \gamma \mathbf{a}^H \mathbf{V}_A \mathbf{T}^H \mathbf{R}_y^{-1} \mathbf{T} \mathbf{V}_A^H \mathbf{a} (\mathbf{a}^H \mathbf{V}_A \mathbf{T}^H \mathbf{R}_y^{-1} \mathbf{T} \mathbf{V}_A^H \mathbf{a}' \\ &\quad + \mathbf{a}'^H \mathbf{V}_A \mathbf{T}^H \mathbf{R}_y^{-1} \mathbf{T} \mathbf{V}_A^H \mathbf{a}). \end{aligned} \quad (59)$$

And, the elements in the bracket in (59) can be simplified as

$$\begin{aligned} &\mathbf{a}^H \mathbf{V}_A \mathbf{T}^H \mathbf{R}_y^{-1} \mathbf{T} \mathbf{V}_A^H \mathbf{a}' \\ &= \mathbf{a}^H \mathbf{V}_A \mathbf{T}^H \left(\mathbf{Q}^{-1} - \frac{\mathbf{Q}^{-1} \mathbf{T} \mathbf{V}_A^H \mathbf{a} \mathbf{a}^H \mathbf{V}_A \mathbf{T}^H \mathbf{Q}^{-1}}{\gamma^{-1} + \mathbf{a}^H \mathbf{B} \mathbf{a}} \right) \\ &\quad \times \mathbf{T} \mathbf{V}_A^H \mathbf{a}' \\ &= j \frac{2\pi}{\lambda} \cos \theta_0 \left(1 - \frac{\mathbf{a}^H \mathbf{B} \mathbf{a}}{\gamma^{-1} + \mathbf{a}^H \mathbf{B} \mathbf{a}} \right) \mathbf{a}^H \mathbf{B} \mathbf{D} \mathbf{a}. \end{aligned} \quad (60)$$

and

$$\begin{aligned} &\mathbf{a}'^H \mathbf{V}_A \mathbf{T}^H \mathbf{R}_y^{-1} \mathbf{T} \mathbf{V}_A^H \mathbf{a} \\ &= \mathbf{a}'^H \mathbf{V}_A \mathbf{T}^H \left(\mathbf{Q}^{-1} - \frac{\mathbf{Q}^{-1} \mathbf{T} \mathbf{V}_A^H \mathbf{a} \mathbf{a}^H \mathbf{V}_A \mathbf{T}^H \mathbf{Q}^{-1}}{\gamma^{-1} + \mathbf{a}^H \mathbf{B} \mathbf{a}} \right) \\ &\quad \times \mathbf{T} \mathbf{V}_A^H \mathbf{a} \\ &= -j \frac{2\pi}{\lambda} \cos \theta_0 \left(1 - \frac{\mathbf{a} \mathbf{B} \mathbf{a}}{\gamma^{-1} + \mathbf{a} \mathbf{B} \mathbf{a}} \right) \mathbf{a}^H \mathbf{D} \mathbf{B} \mathbf{a}, \end{aligned} \quad (61)$$

respectively. Obviously, $\mathbf{B} \mathbf{D} = \mathbf{D} \mathbf{B}$, hence we can conclude that $\mathbf{F}_{\gamma, \theta_0} = 0$. In addition,

$$\begin{aligned} \mathbf{F}_{\theta_0, \gamma} &= \mathbf{Tr} \left\{ \mathbf{R}_y^{-1} \frac{\partial \mathbf{R}_y}{\partial \theta_0} \mathbf{R}_y^{-1} \frac{\partial \mathbf{R}_y}{\partial \gamma} \right\} \\ &= \mathbf{Tr} \left\{ \mathbf{R}_y^{-1} \frac{\partial \mathbf{R}_y}{\partial \gamma} \mathbf{R}_y^{-1} \frac{\partial \mathbf{R}_y}{\partial \theta_0} \right\} \\ &= \mathbf{F}_{\gamma, \theta_0} = 0. \end{aligned} \quad (62)$$

Finally, the $\mathbf{F}_{\theta_0, \theta_0}$ can be written as (63) at the bottom of this page, where

$$F_a = (\mathbf{a}^H \mathbf{V}_A \mathbf{T}^H \mathbf{R}_y^{-1} \mathbf{T} \mathbf{V}_A^H \mathbf{a}')^2, \quad (64)$$

$$F_b = (\mathbf{a}^H \mathbf{V}_A \mathbf{T}^H \mathbf{R}_y^{-1} \mathbf{T} \mathbf{V}_A^H \mathbf{a}) (\mathbf{a}'^H \mathbf{V}_A \mathbf{T}^H \mathbf{R}_y^{-1} \mathbf{T} \mathbf{V}_A^H \mathbf{a}') \quad (65)$$

and

$$F_c = (\mathbf{a}'^H \mathbf{V}_A \mathbf{T}^H \mathbf{R}_y^{-1} \mathbf{T} \mathbf{V}_A^H \mathbf{a})^2. \quad (66)$$

Then, the component of F_a can be simplified as (60), where \mathbf{D} can be rewritten in Kronecker product form as

$$\mathbf{D} = \mathbf{I}_{M_s} \otimes \mathbf{D}_a + \mathbf{D}_s \otimes \mathbf{I}_{M_a} \quad (67)$$

where

$$\mathbf{D}_a = \begin{bmatrix} d_{1,1} & 0 & \cdots & 0 \\ 0 & d_{1,2} & \cdots & 0 \\ \vdots & \vdots & \ddots & \vdots \\ 0 & 0 & \cdots & d_{1,M_a} \end{bmatrix} \quad (68)$$

and

$$\mathbf{D}_s = \begin{bmatrix} d_{1,1} & 0 & \cdots & 0 \\ 0 & d_{2,1} & \cdots & 0 \\ \vdots & \vdots & \ddots & \vdots \\ 0 & 0 & \cdots & d_{M_s,1} \end{bmatrix}. \quad (69)$$

Thus, $\mathbf{a}^H \mathbf{B} \mathbf{D} \mathbf{a}$ can be given by

$$\begin{aligned}
& \mathbf{a}^H \mathbf{B} \mathbf{D} \mathbf{a} \\
&= \frac{1}{M_a} (\mathbf{a}_s \otimes \mathbf{a}_a)^H (\mathbf{C} \otimes \mathbf{1}_{M_a} \mathbf{1}_{M_a}^H) (\mathbf{I}_{M_s} \otimes \mathbf{D}_a \\
&\quad + \mathbf{D}_s \otimes \mathbf{I}_{M_a}) (\mathbf{a}_s \otimes \mathbf{a}_a) \\
&= \frac{1}{M_a} (\mathbf{a}_s^H \mathbf{C} \mathbf{a}_s \otimes \mathbf{a}_a^H \mathbf{1}_{M_a} \mathbf{1}_{M_a}^H \mathbf{D}_a \mathbf{a}_a \\
&\quad + \mathbf{a}_s^H \mathbf{C} \mathbf{D}_s \mathbf{a}_s \otimes \mathbf{a}_a^H \mathbf{1}_{M_a} \mathbf{1}_{M_a}^H \mathbf{a}_a) \\
&= \frac{1}{M_a} \left[\xi \zeta^H \sum_{m_a=1}^{M_a} d_{1,m_a} e^{j \frac{2\pi}{\lambda} d_{1,m_a} \sin \theta_0} \right. \\
&\quad \left. + \left(\sum_{m_s=1}^{M_0} d_{m_s,1} + \frac{\alpha^2}{\alpha^2 + \sigma_q^2} \sum_{m_s=M_0+1}^{M_s} d_{m_s,1} \right) \|\zeta\|^2 \right] \\
&= \frac{1}{M_a} (\xi \zeta^H \Gamma + \mu \|\zeta\|^2), \tag{70}
\end{aligned}$$

where

$$\Gamma = \sum_{m_a=1}^{M_a} d_{1,m_a} e^{j \frac{2\pi}{\lambda} d_{1,m_a} \sin \theta_0} \tag{71}$$

and

$$\mu = \sum_{m_s=1}^{M_0} d_{m_s,1} + \frac{\alpha^2}{\alpha^2 + \sigma_q^2} \sum_{m_s=M_0+1}^{M_s} d_{m_s,1}. \tag{72}$$

Substituting (56) and (70) into (60) yields

$$\begin{aligned}
F_a &= (\mathbf{a}^H \mathbf{V}_A \mathbf{T}^H \mathbf{R}_y^{-1} \mathbf{T} \mathbf{V}_A^H \mathbf{a}')^2 \\
&= -\frac{4\pi^2 \cos^2 \theta_0 (\xi \zeta^H \Gamma + \mu \|\zeta\|^2)^2}{\lambda^2 (\gamma \xi \|\zeta\|^2 + M_a)^2}. \tag{73}
\end{aligned}$$

Furthermore, we can represent the $\mathbf{a}^H \mathbf{D} \mathbf{B} \mathbf{a}$ as follows

$$\begin{aligned}
& \mathbf{a}^H \mathbf{D} \mathbf{B} \mathbf{a} \\
&= \frac{1}{M_a} (\mathbf{a}_s \otimes \mathbf{a}_a)^H (\mathbf{I}_{M_s} \otimes \mathbf{D}_a + \mathbf{D}_s \otimes \mathbf{I}_{M_a}) \\
&\quad (\mathbf{C} \otimes \mathbf{1}_{M_a} \mathbf{1}_{M_a}^H) (\mathbf{a}_s \otimes \mathbf{a}_a) \\
&= \frac{1}{M_a} (\mathbf{a}_s^H \mathbf{C} \mathbf{a}_s \otimes \mathbf{a}_a^H \mathbf{D}_a \mathbf{1}_{M_a} \mathbf{1}_{M_a}^H \mathbf{a}_a + \mathbf{a}_s^H \mathbf{D}_s \mathbf{C} \mathbf{a}_s \\
&\quad \otimes \mathbf{a}_a^H \mathbf{1}_{M_a} \mathbf{1}_{M_a}^H \mathbf{a}_a) \\
&= \frac{1}{M_a} (\xi \zeta \Gamma^H + \mu \|\zeta\|^2). \tag{74}
\end{aligned}$$

Hence, F_c is given by

$$\begin{aligned}
F_c &= (\mathbf{a}^H \mathbf{V}_A \mathbf{T}^H \mathbf{R}_y^{-1} \mathbf{T} \mathbf{V}_A^H \mathbf{a}')^2 \\
&= -\frac{4\pi^2 \cos^2 \theta_0 (\xi \zeta \Gamma^H + \mu \|\zeta\|^2)^2}{\lambda^2 (\gamma \xi \|\zeta\|^2 + M_a)^2}. \tag{75}
\end{aligned}$$

Now, to obtain the F_b , we should derive the expression of $\mathbf{a}^H \mathbf{V}_A \mathbf{T}^H \mathbf{R}_y^{-1} \mathbf{T} \mathbf{V}_A^H \mathbf{a}'$ firstly, which can be calculated by

$$\begin{aligned}
& \mathbf{a}^H \mathbf{V}_A \mathbf{T}^H \mathbf{R}_y^{-1} \mathbf{T} \mathbf{V}_A^H \mathbf{a}' \\
&= \mathbf{a}^H \mathbf{V}_A \mathbf{T}^H \left(\mathbf{Q}^{-1} - \frac{\mathbf{Q}^{-1} \mathbf{T} \mathbf{V}_A^H \mathbf{a} \mathbf{a}^H \mathbf{V}_A \mathbf{T}^H \mathbf{Q}^{-1}}{\gamma^{-1} + \mathbf{a}^H \mathbf{B} \mathbf{a}} \right) \\
&\quad \times \mathbf{T} \mathbf{V}_A^H \mathbf{a}' \\
&= \mathbf{a}^H \mathbf{B} \mathbf{a} - \frac{(\mathbf{a}^H \mathbf{B} \mathbf{a})^2}{\gamma^{-1} + \mathbf{a}^H \mathbf{B} \mathbf{a}} \\
&= \frac{\xi \|\zeta\|^2}{\gamma \xi \|\zeta\|^2 + M_a} \tag{76}
\end{aligned}$$

Afterwards, the second item of F_b is derived as

$$\begin{aligned}
& \mathbf{a}'^H \mathbf{V}_A \mathbf{T}^H \mathbf{R}_y^{-1} \mathbf{T} \mathbf{V}_A^H \mathbf{a}' \\
&= \mathbf{a}'^H \mathbf{V}_A \mathbf{T}^H \left(\mathbf{Q}^{-1} - \frac{\mathbf{Q}^{-1} \mathbf{T} \mathbf{V}_A^H \mathbf{a} \mathbf{a}^H \mathbf{V}_A \mathbf{T}^H \mathbf{Q}^{-1}}{\gamma^{-1} + \mathbf{a}^H \mathbf{B} \mathbf{a}} \right) \\
&\quad \times \mathbf{T} \mathbf{V}_A^H \mathbf{a}' \\
&= \frac{4\pi^2}{\lambda^2} \cos^2 \theta_0 \left[\mathbf{a}^H \mathbf{D} \mathbf{B} \mathbf{D} \mathbf{a} - \frac{(\mathbf{a}^H \mathbf{D} \mathbf{B} \mathbf{a})(\mathbf{a}^H \mathbf{B} \mathbf{D} \mathbf{a})}{\gamma^{-1} + \mathbf{a}^H \mathbf{B} \mathbf{a}} \right]. \tag{77}
\end{aligned}$$

Thus, we just need to derive the $\mathbf{a}^H \mathbf{D} \mathbf{B} \mathbf{D} \mathbf{a}$, which can be given by

$$\begin{aligned}
& \mathbf{a}^H \mathbf{D} \mathbf{B} \mathbf{D} \mathbf{a} \\
&= \frac{1}{M_a} (\mathbf{a}_s \otimes \mathbf{a}_a)^H (\mathbf{I}_{M_s} \otimes \mathbf{D}_a + \mathbf{D}_s \otimes \mathbf{I}_{M_a}) \\
&\quad (\mathbf{C} \otimes \mathbf{1}_{M_a} \mathbf{1}_{M_a}^H) (\mathbf{I}_{M_s} \otimes \mathbf{D}_a + \mathbf{D}_s \otimes \mathbf{I}_{M_s}) (\mathbf{a}_s \otimes \mathbf{a}_a) \\
&= \frac{1}{M_a} (\mathbf{a}_s^H \mathbf{C} \mathbf{a}_s \otimes \mathbf{a}_a^H \mathbf{D}_a \mathbf{1}_{M_a} \mathbf{1}_{M_a}^H \mathbf{D}_a \mathbf{a}_a + \mathbf{a}_s^H \mathbf{C} \mathbf{D}_s \mathbf{a}_s \\
&\quad \otimes \mathbf{a}_a^H \mathbf{D}_a \mathbf{1}_{M_a} \mathbf{1}_{M_a}^H \mathbf{a}_a + \mathbf{a}_s^H \mathbf{D}_s \mathbf{C} \mathbf{a}_s \otimes \mathbf{a}_a^H \mathbf{1}_{M_a} \mathbf{1}_{M_a}^H \mathbf{D}_a \mathbf{a}_a \\
&\quad + \mathbf{a}_s^H \mathbf{D}_s \mathbf{C} \mathbf{D}_s \mathbf{a}_s \otimes \mathbf{a}_a^H \mathbf{1}_{M_a} \mathbf{1}_{M_a}^H \mathbf{a}_a) \\
&= \frac{1}{M_a} \left[\xi \Gamma^H \Gamma + \mu (\Gamma^H \zeta + \zeta^H \Gamma) + \left(\sum_{m_s=1}^{M_0} d_{m_s,1}^2 \right. \right. \\
&\quad \left. \left. + \frac{\alpha^2}{\alpha^2 + \sigma_q^2} \sum_{m_s=M_0+1}^{M_s} d_{m_s,1}^2 \right) \|\zeta\|^2 \right] \\
&= \frac{1}{M_a} (\xi \|\Gamma\|^2 + 2\mu \Re [\Gamma^H \zeta] + \nu \|\zeta\|^2), \tag{78}
\end{aligned}$$

where

$$\nu = \sum_{m_s=1}^{M_0} d_{m_s,1}^2 + \frac{\alpha^2}{\alpha^2 + \sigma_q^2} \sum_{m_s=M_0+1}^{M_s} d_{m_s,1}^2. \tag{79}$$

Therefore, combining (76), (77) and (78), we have

$$\begin{aligned}
F_b &= (\mathbf{a}^H \mathbf{V}_A \mathbf{T}^H \mathbf{R}_y^{-1} \mathbf{T} \mathbf{V}_A^H \mathbf{a}') (\mathbf{a}'^H \mathbf{V}_A \mathbf{T}^H \mathbf{R}_y^{-1} \mathbf{T} \mathbf{V}_A^H \mathbf{a}') \\
&= \frac{4\pi^2 \xi \|\zeta\|^2}{\lambda^2 M_a (\gamma \xi \|\zeta\|^2 + M_a)} \cos^2 \theta_0 \left(\xi \|\Gamma\|^2 + 2\mu \Re [\Gamma^H \zeta] \right. \\
&\quad \left. + \nu \|\zeta\|^2 - \frac{\xi^2 \|\Gamma\|^2 \|\zeta\|^2 + 2\xi \mu \|\zeta\|^2 \Re [\Gamma^H \zeta] + \mu^2 \|\zeta\|^4}{\gamma^{-1} M_a + \xi \|\zeta\|^2} \right) \\
&= \frac{4\pi^2 \cos^2 \theta_0 \xi \|\zeta\|^2}{\lambda^2 (\gamma \xi \|\zeta\|^2 + M_a)^2} \left[\xi \|\Gamma\|^2 + 2\mu \Re [\Gamma^H \zeta] \right. \\
&\quad \left. + \nu \|\zeta\|^2 + \frac{\gamma \|\zeta\|^4}{M_a} (\xi \nu - \mu^2) \right]. \tag{80}
\end{aligned}$$

Finally, substitute the (73), (75) and (80) into (63), $\mathbf{F}_{\theta_0, \theta_0}$ is given by

$$\begin{aligned}
\mathbf{F}_{\theta_0, \theta_0} &= \gamma^2 (F_a + 2F_b + F_c) \\
&= \frac{8\pi^2 \gamma^2 \cos^2 \theta_0}{\lambda^2 M_a (\gamma \xi \|\zeta\|^2 + M_a)^2} \\
&\quad \times \left[\|\zeta\|^4 (\xi \nu - \mu^2) (\gamma \xi \|\zeta\|^2 + M_a) \right. \\
&\quad \left. + M_a \xi^2 (\|\zeta\|^2 \|\Gamma\|^2 - \Re [(\Gamma^H \zeta)^2]) \right]. \tag{81}
\end{aligned}$$

Now, we complete the derivation for the closed-form expression of the FIM for the HAD architecture with mixed-ADCs.

REFERENCES

- [1] T. E. Tuncer and B. Friedlander, *Classical and Modern Direction-of-Arrival Estimation*. Academic Press, 2009.
- [2] J. Hu, F. Shu, and J. Li, "Robust synthesis method for secure directional modulation with imperfect direction angle," *IEEE Commun. Lett.*, vol. 20, no. 6, pp. 1084–1087, 2016.
- [3] F. Shu, X. Wu, J. Hu, J. Li, R. Chen, and J. Wang, "Secure and precise wireless transmission for random-subcarrier-selection-based directional modulation transmit antenna array," *IEEE J. Sel. Areas Commun.*, vol. 36, no. 4, pp. 890–904, 2018.
- [4] C. Qian, F. Vincent, Z. Jiang, W. Shilian, and W. Fanggang, "Wfrt-aided power-efficient multi-beam directional modulation schemes based on frequency diverse array," *IEEE Trans. Wireless Commun.*, vol. 18, no. 11, pp. 5211–5226, 2019.
- [5] Y. Zeng and R. Zhang, "Energy-efficient UAV communication with trajectory optimization," *IEEE Trans. Wireless Commun.*, vol. 16, no. 6, pp. 3747–3760, 2017.
- [6] N. Kaur and S. K. Sood, "An energy-efficient architecture for the internet of things (IoT)," *IEEE Systems Journal*, vol. 11, no. 2, pp. 796–805, 2017.
- [7] S. Hong, C. Pan, H. Ren, K. Wang, and A. Nallanathan, "Artificial-noise-aided secure MIMO wireless communications via intelligent reflecting surface," *IEEE Trans. Commun.*, vol. 68, no. 12, pp. 7851–7866, 2020.
- [8] Q. Wu and R. Zhang, "Beamforming optimization for wireless network aided by intelligent reflecting surface with discrete phase shifts," *IEEE Trans. Commun.*, vol. 68, no. 3, pp. 1838–1851, 2020.
- [9] C. Pan, H. Ren, K. Wang, W. Xu, M. ElKashlan, A. Nallanathan, and L. Hanzo, "Multicell MIMO communications relying on intelligent reflecting surfaces," *IEEE Trans. Wireless Commun.*, vol. 19, no. 8, pp. 5218–5233, 2020.
- [10] R. Schmidt, "A signal subspace approach to multiple emitter location and spectral estimation," *Ph. D. Dissertation. Stanford Univ.*, 1981.
- [11] A. Barabell, "Improving the resolution performance of eigenstructure-based direction-finding algorithms," in *ICASSP '83. IEEE International Conference on Acoustics, Speech, and Signal Processing*, vol. 8, 1983, pp. 336–339.
- [12] R. Roy, A. Paulraj, and T. Kailath, "ESPRIT—a subspace rotation approach to estimation of parameters of cisoids in noise," *IEEE Transactions on Acoustics, Speech, and Signal Processing*, vol. 34, no. 5, pp. 1340–1342, 1986.
- [13] R. Roy and T. Kailath, "Esprit-estimation of signal parameters via rotational invariance techniques," *IEEE Transactions on Acoustics, Speech, and Signal Processing*, vol. 37, no. 7, pp. 984–995, 1989.
- [14] B. Ottersten, M. Viberg, and T. Kailath, "Performance analysis of the total least squares esprit algorithm," *IEEE Trans. Signal Process.*, vol. 39, no. 5, pp. 1122–1135, 1991.
- [15] M. Pesavento, A. B. Gershman, and M. Haardt, "Unitary root-MUSIC with a real-valued eigendecomposition: a theoretical and experimental performance study," *IEEE Trans. Signal Process.*, vol. 48, no. 5, pp. 1306–1314, 2000.
- [16] F. Yan, M. Jin, S. Liu, and X. Qiao, "Real-valued MUSIC for efficient direction estimation with arbitrary array geometries," *IEEE Trans. Signal Process.*, vol. 62, no. 6, pp. 1548–1560, 2014.
- [17] L. Cheng, Y. Wu, J. Zhang, and L. Liu, "Subspace identification for DOA estimation in massive/full-dimension MIMO systems: Bad data mitigation and automatic source enumeration," *IEEE Trans. Signal Process.*, vol. 63, no. 22, pp. 5897–5909, 2015.
- [18] H. Huang, J. Yang, H. Huang, Y. Song, and G. Gui, "Deep learning for super-resolution channel estimation and DOA estimation based massive MIMO system," *IEEE Trans. Veh. Technol.*, vol. 67, no. 9, pp. 8549–8560, 2018.
- [19] X. Huang and B. Liao, "One-bit MUSIC," *IEEE Signal Process. Lett.*, vol. 26, no. 7, pp. 961–965, 2019.
- [20] H. Lee and C. G. Sodini, "Analog-to-digital converters: Digitizing the analog world," *Proceedings of the IEEE*, vol. 96, no. 2, pp. 323–334, 2008.
- [21] F. Shu, Y. Qin, T. Liu, L. Gui, Y. Zhang, J. Li, and Z. Han, "Low-complexity and high-resolution DOA estimation for hybrid analog and digital massive MIMO receive array," *IEEE Trans. Commun.*, vol. 66, no. 6, pp. 2487–2501, 2018.
- [22] K. Wu, W. Ni, T. Su, R. P. Liu, and Y. J. Guo, "Robust unambiguous estimation of angle-of-arrival in hybrid array with localized analog subarrays," *IEEE Trans. Wireless Commun.*, vol. 17, no. 5, pp. 2987–3002, 2018.
- [23] D. Fan, F. Gao, Y. Liu, Y. Deng, G. Wang, Z. Zhong, and A. Nallanathan, "Angle domain channel estimation in hybrid millimeter wave massive MIMO systems," *IEEE Trans. Wireless Commun.*, vol. 17, no. 12, pp. 8165–8179, 2018.
- [24] S. Li, Y. Liu, L. You, W. Wang, H. Duan, and X. Li, "Covariance matrix reconstruction for doa estimation in hybrid massive mimo systems," *IEEE Wireless Communications Letters*, vol. 9, no. 8, pp. 1196–1200, 2020.
- [25] D. Hu, Y. Zhang, L. He, and J. Wu, "Low-complexity deep-learning-based DOA estimation for hybrid massive MIMO systems with uniform circular arrays," *IEEE Wireless Commun. Lett.*, vol. 9, no. 1, pp. 83–86, 2020.
- [26] J. Singh, O. Dabeer, and U. Madhow, "On the limits of communication with low-precision analog-to-digital conversion at the receiver," *IEEE Trans. Commun.*, vol. 57, no. 12, pp. 3629–3639, 2009.
- [27] L. Fan, S. Jin, C. Wen, and H. Zhang, "Uplink achievable rate for massive MIMO systems with low-resolution ADC," *IEEE Commun. Lett.*, vol. 19, no. 12, pp. 2186–2189, 2015.
- [28] S. Jin, X. Liang, K. Wong, X. Gao, and Q. Zhu, "Ergodic rate analysis for multipair massive MIMO two-way relay networks," *IEEE Trans. Wireless Commun.*, vol. 14, no. 3, pp. 1480–1491, 2015.
- [29] C. Kong, C. Zhong, S. Jin, S. Yang, H. Lin, and Z. Zhang, "Full-duplex massive MIMO relaying systems with low-resolution ADCs," *IEEE Trans. Wireless Commun.*, vol. 16, no. 8, pp. 5033–5047, 2017.
- [30] L. Xu, L. Sun, G. Xia, T. Liu, F. Shu, Y. Zhang, and J. Wang, "Secure hybrid digital and analog precoder for mmWave systems with low-resolution DACs and finite-quantized phase shifters," *IEEE Access*, vol. 7, pp. 109763–109775, 2019.
- [31] B. Shi, N. Chen, X. Zhu, Y. Qian, Y. Zhang, F. Shu, and J. Wang, "Impact of low-resolution ADC on DOA estimation performance for massive MIMO receive array," *arXiv preprint*, vol. arXiv:2011.00451, 2020.
- [32] N. Liang and W. Zhang, "Mixed-ADC massive MIMO," *IEEE J. Sel. Areas Commun.*, vol. 34, no. 4, pp. 983–997, 2016.
- [33] J. Zhang, L. Dai, Z. He, S. Jin, and X. Li, "Performance analysis of mixed-ADC massive MIMO systems over rician fading channels," *IEEE J. Sel. Areas Commun.*, vol. 35, no. 6, pp. 1327–1338, 2017.
- [34] J. Zhang, L. Dai, Z. He, B. Ai, and O. A. Dobre, "Mixed-ADC/DAC multipair massive MIMO relaying systems: Performance analysis and power optimization," *IEEE Trans. Commun.*, vol. 67, no. 1, pp. 140–153, 2019.
- [35] W. Tan, S. Jin, C. Wen, and Y. Jing, "Spectral efficiency of mixed-ADC receivers for massive MIMO systems," *IEEE Access*, vol. 4, pp. 7841–7846, 2016.
- [36] B. Shi, L. Zhu, W. Cai, N. Chen, T. Shen, P. Zhu, F. Shu, and J. Wang, "On performance loss of DOA measurement using massive MIMO receiver with mixed-ADCs," *arXiv preprint*, vol. arXiv:2104.02447, 2021.
- [37] O. Orhan, E. Erkip, and S. Rangan, "Low power analog-to-digital conversion in millimeter wave systems: Impact of resolution and bandwidth on performance," in *2015 Information Theory and Applications Workshop (ITA)*, 2015, pp. 191–198.
- [38] J. Zhu, C. Wen, J. Tong, C. Xu, and S. Jin, "Grid-less variational bayesian channel estimation for antenna array systems with low resolution ADCs," *IEEE Trans. Wireless Commun.*, vol. 19, no. 3, pp. 1549–1562, 2020.
- [39] S. Cui, A. J. Goldsmith, and A. Bahai, "Energy-constrained modulation optimization," *IEEE Trans. Wireless Commun.*, vol. 4, no. 5, pp. 2349–2360, 2005.
- [40] X. Gao, L. Dai, S. Han, C. I, and R. W. Heath, "Energy-efficient hybrid analog and digital precoding for mmwave MIMO systems with large antenna arrays," *IEEE J. Sel. Areas Commun.*, vol. 34, no. 4, pp. 998–1009, 2016.
- [41] C. He, B. Sheng, P. Zhu, and X. You, "Energy efficient comparison between distributed MIMO and co-located MIMO in the uplink cellular systems," in *2012 IEEE Vehicular Technology Conference (VTC Fall)*, 2012, pp. 1–5.
- [42] R. A. Horn and C. R. Johnson, *Matrix Analysis*. Cambridge University Press, 2012.